Article

Immunomagnetic Separation of Microorganisms with Iron Oxide Nanoparticles

Julian A. Thomas, Florian Schnell, Yasmin Kaveh-Baghbaderani[iD]**, Sonja Berensmeier**[iD] **and Sebastian P. Schwaminger** *[iD]

Bioseparation Engineering Group, Department of Mechanical Engineering, Technical University of Munich, 85748 Garching, Germany; julian.thomas@bayern-mail.de (J.A.T.); fschnell.private@gmail.com (F.S.); y.kaveh@tum.de (Y.K.-B.); s.berensmeier@tum.de (S.B.)

* Correspondence: s.schwaminger@tum.de; Tel.: +49-89289-15747

check for updates

Abstract: The early detection of Legionella in water reservoirs, and the prevention of their often fatal diseases, requires the development of rapid and reliable detection processes. A method for the magnetic separation (MS) of *Legionella pneumophila* by superparamagnetic iron oxide nanoparticles is developed, which represents the basis for future bacteria detection kits. The focus lies on the separation process and the simplicity of using magnetic nanomaterials. Iron oxide nanoparticles are functionalized with epoxy groups and *Legionella*-specific antibodies are immobilized. The resulting complexes are characterized with infrared spectroscopy and tested for the specific separation and enrichment of the selected microorganisms. The cell-particle complexes can be isolated in a magnetic field and detected with conventional methods such as fluorescence detection. A nonspecific enrichment of bacteria is also possible by using bare iron oxide nanoparticles (BIONs), which we used as a reference to the nanoparticles with immobilized antibodies. Furthermore, the immunomagnetic separation can be applied for the detection of multiple other microorganisms and thus might pave the way for simpler bacterial diagnosis.

Keywords: magnetic nanoparticles; iron oxide nanoparticles; immunoassay; magnetic separation; microorganism detection; nanoparticle functionalization; antibody immobilization

1. Introduction

Fast bacterial separation methods are crucial for diagnostics, and the development of rapid detection and quantification devices. Novel methodologies are needed and can reduce the diagnostic time and thus allow faster treatment. *Legionella pneumophila* is a pathogen, which causes Legionnaire's disease, which are quite difficult to cultivate, which leads to detection times for contaminated water sources of up to 14 days. This timeframe should be reduced since Legionnaire's disease is an "avoidable" disease, which is not passed on from person to person but which is fatal in 5–40% of cases [1,2]. In addition to detection in water, the rapid and accurate detection of *Legionella* in body fluids is essential for early medical diagnosis. To date, 50 Legionella species and more than 70 serogroups are known. More than 90% of the cases of legionnaire's disease are caused by *Legionella pneumophila* which is a rod-shaped bacterium with 0.4–1.5 μm diameter and up to 6 mm length [1,3]. The standardized cultivation of *Legionella* is regulated internationally by ISO 11371. The typical determination of a *Legionella* contamination is based on the sampling of 100–1000 mL water and the cultivation of the microorganisms on a GVPC (Glycine Vancomycin Polymyxin Cycloheximide) agar, which takes 10 to 14 days due to the long doubling time of *Legionella pneumophila* in order to determine the limit value of 100 colony forming unit in 100 mL of water. While this quite time-consuming technique still represents the state of the art, faster processes have been reported but are often either quite complicated

or expensive [4–6]. These methods include fluorescent antibody staining, antigen detection, serological testing and polymerase chain reaction (PCR) [5,7]. Filtration, centrifugation, and immunomagnetic separation (IMS) techniques can be used to concentrate bacteria and are often necessary in order to achieve a higher detectability of the pathogens and to condition the samples [8–10]. Pre-purification steps are essential in the separation of *Legionella* from greywater [11]. The separation of a sample mixture by IMS can significantly accelerate the detection process by concentrating the target bacterium and removing interfering substances [12]. For this, neither expensive sophisticated equipment nor scientific knowhow is required. IMS is based on the separation of adsorbent from the liquid phase in a magnetic field. Thus, superparamagnetic iron oxide nanomaterials with a high specific surface area are a promising adsorbent material. Bare iron oxide nanoparticles (BIONs) with 5–50 nm size can be used for e.g. protein purification [13,14], enzyme immobilization [15] and harvesting of algae [16]. Usually, the nanoparticles are embedded in polymers and used as superparamagnetic microbeads (0.1–100 μm) and are further modified with functional group to anchor an immunoactive group, such as an antibody [17]. The immobilized antibody needs to be specific to the respective epitope on the surface of *Legionella pneumophila*. Subsequent fluorescence analysis e.g. with a fluorescent-labelled antibody offers the potential for rapid and accurate quantification [18]. In the long term, a kit could be developed that enables the detection of *Legionella* by untrained staff on site and in a few hours.

Similar approaches either use magnetic beads which recognize antibodies coupled to the *Legionella pneumophila* [19,20], or, a cell-specific antibody coupled to the magnetic beads [18,21]. Bloemen et al. used 5–25 μm sized PEG-coated magnetic beads with immobilized antibodies for the separation of *Legionella* and needed a contact time of 1 h [21]. The particle size significantly influences the separation efficiency. Of crucial importance in the evaluation of a separation process is the recovery rate, which relates to amount of cells which are successfully separated from the original solution. Using commercial MACS®microbeads coated with monoclonal mouse anti-FITC antibodies, Füchslin et al. reached a separation efficiency of 95% of the *Legionella* in an aqueous suspension. Then, 92% *Legionella* cells could be separated from a cell mixture with *Escherichia coli*, while only adsorbing below 1% of *E. coli* cells [19]. Other approaches to separate *Legionella* include self-synthesized Fe_3O_4-gold-particles and commercial streptavidin-coated magnetic nanoparticles [22].

The goal of this work is the successful functionalization of magnetic nanoparticles with antibodies for the separation of the bacteria in an aqueous medium. The magnetic nanoparticles used for the immobilization of antibodies are synthesized and characterized for the present work. For this purpose, the size of particles were determined with dynamic light scattering (DLS), the zeta potential was investigated as a function of the pH-value, and an analysis of the crystal structure was carried out with X-ray diffraction (XRD). The success of the coating and coupling processes is verified by IR spectroscopy. Furthermore, the magnetization of the particles is investigated. Magnetic separation can be used as a preliminary step for subsequent filtration or direct detection using further labelling or cultivation. The elaborated separation method was tested for its transferability to the separation of other cell types and its specificity to *Legionella*. Therefore, we compared the nanoparticles with bare iron oxide nanoparticles (BIONs). Since even those non-functionalized nanoparticles show a high binding affinity, we further tested the influence of pH on the enrichment of bacteria. The aim is a quick and easy separation and enrichment process, which nevertheless provides reliable qualitative results.

2. Materials and Methods

2.1. Synthesis

In accordance with Roth et al., 35.0 g of iron (II) chloride and 86.4 g of iron (III) chloride, obtained from Sigma-Aldrich, were dissolved and mixed in 200 mL of deionized water [23]. 1 M NaOH (Fluka) was prepared with deionized water and filled in a stirred tank glass reactor under a nitrogen atmosphere [23]. Subsequently, the salt solution was added dropwise, which immediately forms a black precipitate. After complete addition, the reaction was continued for half an hour under constant

conditions. The resulting particles were washed several times with deionized water until a conductivity of less than 200 µS/cm was reached.
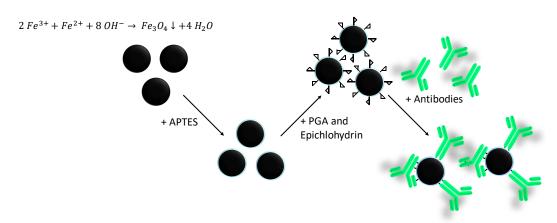
2.2. Coating

BIONs (1 g) are dispersed in 300 mL of ethanol in a round bottom flask and sonicated for 1 h. After the addition of 3-aminopropyltriethoxysilane (APTES) followed the mixture was treated another hour in an ultrasonic bath. The reaction product was dispersed four times in ethanol for washing and then separated magnetically. It was then washed in water until a conductivity of less than 200 µS/cm was measured. Subsequently, 25 mg of the functionalized particles were mixed with 2 mL of 2% (v/v) glutaraldehyde. A pH value of 11 was set by titration of 0.5 M NaOH. During the titration, the solution is stirred constantly for 1 h. The resulting polyglutaraldehyde (PGA)-coated particles were washed ten times in water, twice in 1 M NaCl solution, and another two times in water. The complete washing process was repeated twice.

The washed particles were then suspended at a concentration of 25 g/L in a solution of 0.5 M NaOH, 19 mM $NaBH_4$, and 5% (v/v) epichlorhydrin. The mixture reacts under continuous stirring for 6 h. During the reaction, epichlorhydrin binds to the oxygen of the aldehyde and epoxy groups are formed. Afterwards, the product was washed eight times with deionized water and twice with a buffer solution (20 mM NaH_2PO_4, 1.0 M NaCl, pH = 6.8). Until further use, the particles were stored at 4 °C in the same buffer solution. The PGA-coated particles with functional epoxy groups are called @Epoxy in the further text.

2.3. Particle Antibody Coupling

Specific rabbit anti-*Legionella* antibodies (PA1-7227) from Thermo Fisher Scientific are immobilized on @Epoxy particles. The coupling is achieved by direct contact between nanoparticles and proteins. The antibodies are coupled through the epoxy group to the @Epoxy particles. To determine the amount of antibody that can be bound by the coated nanoparticles, an adsorption test was performed with bovine serum albumin and antibodies, which yielded optimal binding conditions at 0.2 mg/mL for a nanoparticle concentration of 1 mg/mL. Thus, for the bacterial enrichment experiments, 1 mL of antibody suspension (c = 0.2 mg/mL) was added to 1 mg nanoparticles. After incubation with heat-inactivated *Legionella*, obtained from BacTrace GmbH, the particle fraction is centrifuged off and the residual concentration of Ab in the supernatant is measured by two methods. A bicinchoninic acid (BCA) assay was carried out to determine the protein concentration. In addition, samples were analyzed by UV/vis spectroscopy at 230 nm and 280 nm.

The whole synthesis, coating, functionalization, and antibody coupling procedure is illustrated in Scheme 1.

$$2\,Fe^{3+} + Fe^{2+} + 8\,OH^- \rightarrow Fe_3O_4 \downarrow + 4\,H_2O$$

Scheme 1. Schematic illustration of the iron oxide synthesis, APTES coating, polyglutaraldehyde (PGA) functionalization, epichlorhydrin activation, and antibody coupling.
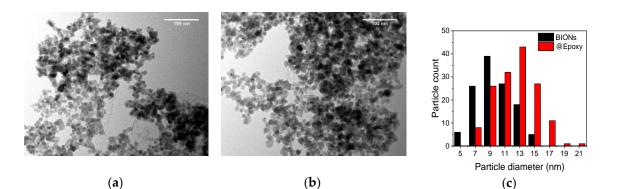
2.4. Characterization

Dynamic light scattering (DLS) and zeta potential measurements were performed with a Beckman Coulter Delsa Nano C Particle Analyzer. The pH is varied by titration of 0.1 M HCl and 0.1 M NaOH. The characterizations are typically performed at a concentration of 1 g/L of nanoparticles in deionized water. The Fourier-transform infrared spectra (FTIR) were measured using a Bruker ALPHA II FTIR spectrometer and the matching Platinum attenuated total reflection (ATR) module. Sixty-four scans per sample and measurement were performed and a baseline was subtracted via the rubber band method in the software OPUS. Transmission electron microscopy (TEM) was carried out with the JEM 1400 Plus microscope from JEOL and the recorded images were subsequently evaluated using ImageJ software. Diluted nanoparticle suspensions were precipitated on carbon copper grids prior to TEM measurements. Around 100 particles per nanoparticle type were measured. X-ray diffraction (XRD) was recorded with a STOE Stadi P diffractometer with a molybdenum radiation source from STOE and Cie. The freeze-dried samples were mounted in transmission geometry and measured while rotating. The magnetic susceptibility of the nanoparticles is determined by a SQUID characterization. For this work, the Quantum Design MPMS 5XL SQUID magnetometer was used. The measurements were carried out at 300 K in magnetic fields varying between −50 kOe to 50 kOe.

2.5. Binding of Cells to the Nanoparticles

Next, 0.8 mg/mL magnetic nanoparticles were added to the cell suspension in phosphate buffered saline (PBS) buffer (20 mM NaH_2PO_4, 1.0 M NaCl, pH = 6.8) and incubated in a shaker for at least 1 h. Depending on the nature of the particles and the use of antibodies, different amounts of cells were bound and magnetically separated. In the case of antibody-particle complexes, 0.1 $g_{Ab}/g_{Particles}$ were used. The number of bound cells were determined by measuring the absorbance at 600 nm in the supernatant. To estimate the number of cells that can be separated by BIONs, a series of experiments with different nanoparticle concentrations were performed. The nanoparticles are added to 1 mL samples of suspensions of *E. coli* BL21(DE3) with an optical density of 0.2. This corresponds to 5×10^7 cells [24]. The mass of BIONs varied from 0.4 mg to 16 mg. In order to investigate the specificity of the antibodies, 0.8 mg @Epoxy+Ab complexes were added to each 1 mL of different cell suspensions (*E. coli*, *Legionella pneumophila*, OD_{600} = 0.2). After 1 h coupling, the particle fraction was separated magnetically. To examine the influence of the pH on the magnetic separation, in each case 1 mL of the PBS buffered (20 mM) *E. coli* was centrifuged off and resuspended in a series of buffers of different pH values. Subsequently, 16 mg of BIONs were added, which are dissolved in 1 mL of the same buffer. The mixture is incubated for 1 h in a shaker at room temperature. Subsequently, the cell-particle complexes are magnetically separated over 1 h. The absorbance of the supernatant is measured. In addition, the OD_{600} of analogously prepared suspensions without nanoparticles were measured. Incubation experiments were performed in triplicates.
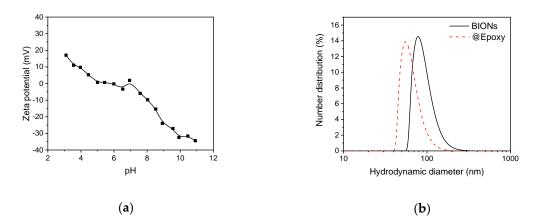
3. Results and Discussion

Nanoparticles are characterized towards their size and material properties in order to facilitate a proper immunomagnetic separation. Figure 1 shows images of the particles taken via TEM. The frequency distributions are in good agreement with previous measurements of magnetite particles [15,21,25–27]. Here, the actual dimensions of the individual particles can be determined optically, whereas dynamic light scattering yields the hydrodynamic diameter of agglomerates [17]. The BIONs show an approximately Gaussian size distribution with a maximum around 10 nm, while the coated and polyglutaraldehyde activated nanoparticles show a broader size distribution with a higher maximum around 12 nm. The difference between the TEM diameters can be related to the thickness of the coating.

(a)   (b)   (c)

Figure 1. Transmission electron microscopy (TEM)-microphotography of bare iron oxide nanoparticles (BIONs) (**a**) and of @Epoxy particles (**b**). Frequency distribution of pure BIONs and PGA-coated SPIONs with various particle diameters, measured by TEM (**c**).

Aside from the size of nanoparticles, hydrodynamic properties play an important role for the further coating process and the functionalization of iron oxide nanoparticles with antibodies. Figure 2a shows a dynamic measurement of the zeta potential of pure uncoated nanoparticles. The potential reaches values from +17.04 mV at pH = 3.1 up to −34.42 mV at pH = 10.91. The isoelectric point of BIONs is at about pH = 6, which matches the results of Bini et al. and Schwaminger et al. [27,28].

(a)   (b)

Figure 2. (**a**) Zeta potential of BIONs at various pH-values titrated from pH 3 to pH 11 with sodium hydroxide (0.1 M). (**b**) Size distribution of coated @Epoxy and uncoated BIONs, determined by dynamic light scattering (DLS) at pH 10.

The charge of the particles can be explained by hydroxyl groups on the surface of the BIONs. These can be detected by FTIR spectroscopy. In the basic range, the Fe-OH group dissociates to form Fe-O$^-$. In the acidic range, a proton is taken up and Fe-OH$_2^+$ is formed [29]. The stabilization of nanoparticles at alkaline pH values is necessary in order to obtain a homogeneous coating and thus a further functionalization with APTES. Stable non-agglomerated BIONs form the basis of the further functionalization and antibody immobilization. APTES coated nanoparticles show a zeta potential of 17.59 at pH 6.4 and the @EpoxyPGA functionalized nanoparticles possess a zeta potential of −23.88 at pH 7.3, which further indicates a successful coating and functionalization.
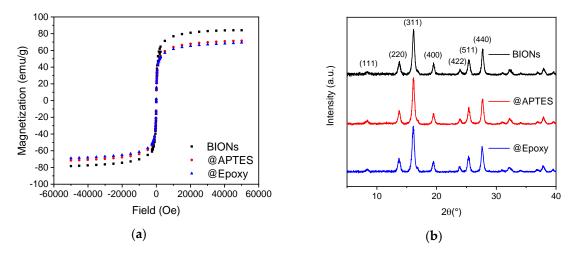
Figure 2b shows the DLS-measured size distribution of the BIONs at pH 10, where the nanoparticles are colloidally stable with aggregated structures of ~80 nm size and possess a high zeta potential (>30 mV) [25].

The silica coating and the polyglutaraldehyde activation stabilize the particles against agglomeration, which explains the smaller hydrodynamic diameters (~55 nm). The stabilization is caused by the mutual repulsion of electrostatically charged particles [28].

Nevertheless, the values measured for the coated particles overestimate the actual particle diameter. This is due to still-existing agglomeration effects, and liquid boundary layers, which surround the particles in the aqueous phase. A more accurate determination of the average size of a single particle is possible by TEM [26].

The functionality of a magnetic separation process is not only dependent on the functionalization but also on a high magnetization at elevated magnetic fields and superparamagnetic properties of the nanomaterials, which allow the manipulation in magnetic fields.
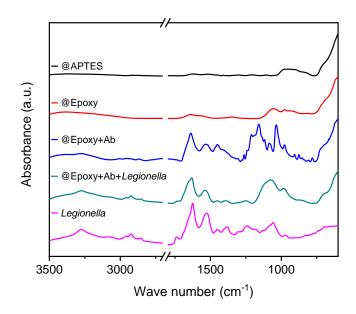
Figure 3a shows the typical sigmoidal curves of superparamagnetic nanoparticles in a magnetic field. At an external field of 0 Oe the particles do not possess any remanence (<0.5 emu/g).

Figure 3. (**a**) SQUID-analysis of pure and coated BIONs at 300 K. (**b**) Powder X-ray diffractograms of different nanoparticles.

BIONs reach the highest magnetization with 84.12 emu/g. This coincides with the results of previous measurements [30–32]. The APTES-coated particles reach up to 71.28 emu/g and the @Epoxy particles show a maximum of 68.93 emu/g. The decreasing magnetization is explained by the thin silicon layer on the particle surface after the coating process. A similar effect has been previously reported by McCarthy et al. [32]. The crystal structure of the previously freeze-dried particle powder was examined by XRD. The angles at which the reflections appear suggest the cubic face-centered structure of crystalline magnetite. These can be assigned to the typical crystal planes designated in Figure 3b [33]. Typical maghemite reflections, such as (210) and (211), are not detected [34].

The surface properties of functionalized nanomaterials can be verified spectroscopically with ATR IR spectroscopy. The prominent peak at about 600 cm^{-1} resembles a Fe-O vibration which is typical for Fe_3O_4 (Figure 4). Similar peaks are described by Ma et al. and Yamaura et al. [35,36]. Several small peaks between 700 and 1000 cm^{-1} can be attributed to Si-O vibrations. Examples are the band of the Si-OH group at about 900 cm^{-1} or the band of the Si-O-Si bond between 900 cm^{-1} and 1000 cm^{-1} [35–38] The significant peaks at about 1550 cm^{-1} and 1635 cm^{-1} are attributed to the COO$^-$ group and the C=O bond, respectively. The appearance of these bands indicates a ring opening of the epoxy rings. The characteristic bands of the C-O-C and C-O and C-C ring stretching modes at 1060 cm^{-1}, 1000 cm^{-1}, and 900 cm^{-1} can be seen in the spectrum of @Epoxy particles, indicating a functional epoxy coating [29,37–39].
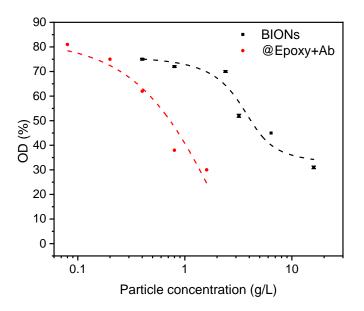
Figure 4. Attenuated total reflection infrared (ATR IR)-spectra of APTES-coated BIONs, @Epoxy nanoparticles with and without immobilized antibodies. The spectra of particles with immobilized antibodies is shown before and after coupling with *Legionella* and the spectrum of *Legionella* is shown.

Considering the spectrum of the antibody-coupled particles in Figure 4, the great number of peaks in the frequency range between 800 cm^{-1} and 1200 cm^{-1} is remarkable and verifies the complete coupling of 0.2 mg$_{Ab}$/mg$_{Particles}$. Absorbance measurements at 230 and 280 nm, and BCA assays of the supernatant are in good agreement with IR spectroscopy data, as we detected no protein. The antibody load achieved for the @Epoxy+Ab particles are an improvement compared to previous studies [21,40]. Bloemen et al. [40] reach between 0.010 and 0.025 g$_{Ab}$/g$_{Particles}$ on magnetite particles with functional COOH groups loadings. The gold coatings of Zhang et al. [41] show a maximum loading of 0.088 g$_{Ab}$/g$_{Particles}$ which is similar to our results.

These are characteristic oscillations of organic compounds, which essentially contain carbon, oxygen, and nitrogen. The peaks, which occur at about 1200 cm^{-1}, can be ascribed to C-O and C-N bonds, and the bands of the C-O-C bond can be observed between 900 cm^{-1} and 1200 cm^{-1} [42,43].

The amide bands appearing at 1550 cm^{-1} and 1650 cm^{-1} indicate coupling [39]. Numerous bands are visible, which influence and overlap one another and make an exact assignment difficult. The spectrum of the *Legionella* used in this work is shown in Figure 4. Subsequently, it is compared with the spectrum of @Epoxy+Ab+*Legionella* complexes. Asymmetric and symmetrical stretching vibrations of the carboxyl group can be observed at about 1605 cm^{-1} and 1391 cm^{-1}, respectively [44]. The first peak is enhanced by overlapping with the amide I band at 1635 cm^{-1}. Other characteristic peaks are the amide II band at 1541 cm^{-1}, which indicates polypeptide structures, and the methyl-diffraction band at 1456 cm^{-1}. The same characteristic peaks at 1100 cm^{-1} and 1250 cm^{-1} appear in the spectrum of pure and particle-coupled *Legionella* samples and confirm a successful coupling process.

We compared the immunomagnetic separation of antibody-coupled particles to BIONs. Figure 5 shows a decrease of the optical density after separation due to bound bacteria. At c (BIONs) = 0.4 g/L, 75% of the starting OD is still present after separation; whereas only 31% are present at c (BIONs) = 16 g/L. For larger concentrations, the polynomial approximated curve flattens out. Thus, a further increase of the particle mass hardly influences the decrease in the optical density.
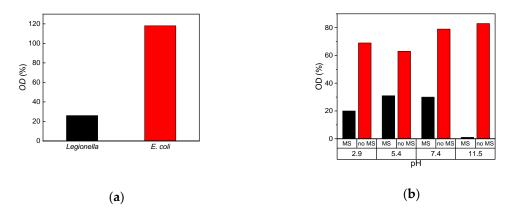
Figure 5. Optical density of the cell suspension after separation related to the density before. Separation by BIONs is compared with separation by @Epoxy+Ab-particle-complexes which have been incubated with Legionella (OD = 0.2 corresponding to 100% or 5×10^7 cells) at pH 7.4 for 1 h. The reference absorbance of water incubated with both nanoparticle species for all particle concentrations (pH 7.4) shows the same value as water after magnetic separation of 1 h (OD = 0).

The optical density of the suspension after magnetic separation is mainly caused by the present cells. Turbidity due to particles is negligible because of their almost complete magnetic separation, which relates to an OD of 0 for the particle reference. The observed separation can be explained by the occurrence of various interactions (van der Waals, electrostatic, acid-base) between cells and particles and is therefore less specific [22].

The high separation rate of about 70% for @Epoxy+Ab and BIONs exceeds the results of previously performed IMS experiments with *E. coli* from Tamer et al. [22]. The optical density of the suspension, which corresponds to the number of Legionella cells, decreases with an increasing nanoparticle concentration. The optical density decreases from 81% when using the lowest up to 30% at the highest @Epoxy+Ab particle concentration (Figure 5). For BIONs, at an about ten times higher concentration of particles compared to @Epoxy+Ab, a similar decrease of the OD is achieved.

The comparison with the separation by BIONs suggests that the interactions between antibodies and Legionella exceed those between pure particles and *E. coli*, as expected from the higher specificity of the binding [35]. In addition, the coated particles have smaller diameters and thus larger specific surface areas [45]. The achieved separation rate of 70% is in line with the achieved rates in previous IMS experiments or even surpasses them [22,46]. However, Füchslin achieved recovery rates of up to 92% using commercial Antibody-coupled MACS®microparticles from Miltenyi Biotec [19]. Since the same separation can be achieved by the addition of a larger number of particles without high-priced antibodies, it is preferable to use BIONs for non-specific separation.

Different cell suspensions are separated by particle complexes made of @Epoxy and *Legionella*-specific antibodies. The resulting optical densities are shown in Figure 6a. A considerable difference between the *Legionella* suspensions and the other samples is visible. Then, 74% of the cells are separated. In the case of. *E. coli* no separation is observed, which verifies the *Legionella*-specificity of @Epoxy+Ab complexes.

(**a**)　　　　　　　　　　　　　　　　　　　　　(**b**)

Figure 6. (**a**) Optical density of the cell suspension after separation with 0.8 g/L @Epoxy+Ab related to the density before (OD 0.2 corresponding to 5×10^7 cells) at pH 7.4. The separation of different cell types by Ab-particle-complexes was compared. The antibodies are specific to *Legionella*. (**b**) Optical density of the cell suspension after separation compared to the OD-value before separation (0.2 corresponding to 5×10^7 cells) in %. The magnetic separation (MS) of *Legionella* with BIONs at different pH values is examined after incubation for 1 h. For comparison, samples without added BIONs for the same incubation time were also examined (no MS).

These observations are consistent with the results of Bloemen et al. and Füchslin et al., who were able to demonstrate a selective separation between *E. coli* and *Legionella* [19,21]. In Füchslin's IMS approach with *Legionella*-specific antibodies only 1% of the present *E. coli* were separated [19].

The high separation efficiency of even bare nanoparticles was our motivation to investigate the behavior of these nanoparticles for bacteria separation. The separation efficiency is strongly dependent on the pH. Electrostatic interactions between the particles and between particles and cells increase with their charge, which is consistent with DLS and zeta potential data. An improved colloidal stabilization leads to a larger effective surface area which is available for cell-particle coupling [44,46]. This explains the improved separation efficiency at higher pH-values (Figure 6b).

These results are quite promising for the development of a process for the concentration of *Legionella pneumophila* prior to detection in water. The time scale with around 1 h of the separation and concentration process is in the range of the requirements for clinical *Legionella* tests in urine, blood, and serum [5,6,47]. The process still demonstrates multiple challenges and the detection limit needs to be improved significantly with fluorescence labelling and accurate detection methods. In the future such a process can provide a sensitive cell enrichment method for *Legionella* detection, which is needed to control drinking water fast and cost-effectively in order to prevent the outbreak of Legionnaires' disease in contaminated resources [48–50].

4. Conclusions

We were able to efficiently couple *Legionella*-specific antibodies via an epoxy ring opening reaction to iron oxide nanoparticles. The successful coupling of $0.2 \text{ mg}_{AB}/\text{g}_{Particle}$ is verified by IR spectroscopy and further immunomagnetic separation. With BIONs, as well as with antibody-modified magnetic nanoparticles complexes, up to 70% of the present *Legionella* cells can be separated, which corresponds to the results of previously developed IMS methods based on magnetic microparticles [19,22,46]. About $16 \text{ mg}_{Particles}/\text{mL}_{cells}$ of BIONs are needed to achieve the same separation as with $0.8 \text{ mg}_{@Epoxy+Ab}/\text{mL}_{cells}$ of antibody-modified nanoparticles.

The specificity of the antibody has great influence on the success of the separation process. Only with highly specific antibodies is the IMS method preferable to separation with pure particles, which is much more cost-efficient. The good performance of pure BIONs allows a comparatively cheap unspecific separation procedure of cells from liquids (magnetic separation, MS) without the use of

antibodies. The increasing stabilization of particle suspensions in basic and acidic environments results in higher separation rates.

Thus, a (selective) pre-separation with magnetic particles and a subsequent concentration for detection by fluorescence assays is suitable. Assuming a sufficiently sensitive analysis, the developed method represents a promising approach for the separation of *Legionella* from liquids. As shown by the example of *E. coli*, the process can also be transferred to other cell types and thus offers a wide range of applications. Other (bio-) molecules, which are interacting with the nanoparticles, could be separated in the same way [12,22].

Magnetic separation might be a decisive technology of the future for bacterial enrichment and therefore for the faster detection of bacteria.

References

1. Fields, B.S.; Benson, R.F.; Besser, R.E. Legionella and Legionnaires' disease: 25 years of investigation. *Clin. Microbiol. Rev.* **2002**, *15*, 506–526. [CrossRef]
2. Phin, N.; Parry-Ford, F.; Harrison, T.; Stagg, H.R.; Zhang, N.; Kumar, K.; Lortholary, O.; Zumla, A.; Abubakar, I. Epidemiology and clinical management of Legionnaires' disease. *Lancet Infect. Dis.* **2014**, *14*, 1011–1021. [CrossRef]
3. Diederen, B.M.W. Legionella spp. and Legionnaires' disease. *J. Infection* **2008**, *56*, 1–12. [CrossRef]
4. Whiley, H.; Taylor, M. Legionella detection by culture and qPCR: Comparing apples and oranges. *Crit. Rev. Microbiol.* **2016**, *42*, 65–74. [CrossRef]
5. Murdoch, D.R. Diagnosis of Legionella infection. *Clin. Infect. Dis.* **2003**, *36*, 64–69. [CrossRef]
6. Pierre, D.M.; Baron, J.; Yu, V.L.; Stout, J.E. Diagnostic testing for Legionnaires' disease. *Ann. Clin. Microbiol. Antimicrob.* **2017**, *16*, 59. [CrossRef]
7. Mercante, J.W.; Winchell, J.M. Current and emerging Legionella diagnostics for laboratory and outbreak investigations. *Clin. Microbiol. Rev.* **2015**, *28*, 95–133. [CrossRef]
8. Bedrina, B.; Macián, S.; Solís, I.; Fernández-Lafuente, R.; Baldrich, E.; Rodríguez, G. Fast immunosensing technique to detect Legionella pneumophila in different natural and anthropogenic environments: Comparative and collaborative trials. *BMC Microbiol.* **2013**, *13*, 88. [CrossRef]
9. Boulanger, C.A.; Edelstein, P.H. Precision and accuracy of recovery of Legionella pneumophila from seeded tap water by filtration and centrifugation. *Appl. Environ. Microbiol.* **1995**, *61*, 1805–1809. [CrossRef]
10. Orrison, L.H.; Cherry, W.B.; Milan, D. Isolation of Legionella pneumophilia from cooling tower water by filtration. *Appl. Environ. Microbiol.* **1981**, *41*, 1202–1205. [CrossRef]
11. Rodríguez-Martínez, S.; Blanky, M.; Friedler, E.; Halpern, M. Legionella spp. isolation and quantification from greywater. *MethodsX* **2015**, *2*, 458–462. [CrossRef]
12. Olsvik, O.; Popovic, T.; Skjerve, E.; Cudjoe, K.S.; Hornes, E.; Ugelstad, J.; Uhlén, M. Magnetic separation techniques in diagnostic microbiology. *Clin. Microbiol. Rev.* **1994**, *7*, 43–54. [CrossRef]

13. Schwaminger, S.P.; Blank-Shim, S.A.; Scheifele, I.; Pipich, V.; Fraga-García, P.; Berensmeier, S. Design of interactions between nanomaterials and proteins: A highly affine peptide tag to bare iron oxide nanoparticles for Magnetic Protein Separation. *Biotechnol. J.* **2019**, *14*, e1800055. [CrossRef]

14. Schwaminger, S.P.; Fraga-García, P.; Blank-Shim, S.A.; Straub, T.; Haslbeck, M.; Muraca, F.; Dawson, K.A.; Berensmeier, S. Magnetic one-step purification of His-tagged protein by bare iron oxide nanoparticles. *ACS Omega* **2019**, *4*, 3790–3799. [CrossRef]

15. Schnell, F.; Kube, M.; Berensmeier, S.; Schwaminger, S.P. Magnetic recovery of cellulase from cellulose substrates with bare iron oxide nanoparticles. *ChemNanoMat* **2019**, *5*, 422–426. [CrossRef]

16. Fraga-García, P.; Kubbutat, P.; Brammen, M.; Schwaminger, S.; Berensmeier, S. Bare iron oxide nanoparticles for magnetic harvesting of microalgae: From interaction behavior to process realization. *Nanomaterials* **2018**, *8*, 292. [CrossRef]

17. Laurent, S.; Forge, D.; Port, M.; Roch, A.; Robic, C.; Vander Elst, L.; Muller, R.N. Magnetic iron oxide nanoparticles: Synthesis, stabilization, vectorization, physicochemical characterizations, and biological applications. *Chem. Rev.* **2008**, *108*, 2064–2110. [CrossRef]

18. Sethi, S.; Gore, M.T.; Sethi, K.K. Increased sensitivity of a direct fluorescent antibody test for Legionella pneumophila in bronchoalveolar lavage samples by immunomagnetic separation based on BioMags. *J. Microbiol. Meth.* **2007**, *70*, 328–335. [CrossRef]

19. Füchslin, H.P.; Kötzsch, S.; Keserue, H.-A.; Egli, T. Rapid and quantitative detection of Legionella pneumophila applying immunomagnetic separation and flow cytometry. *Cytometry Part A* **2010**, *77*, 264–274. [CrossRef]

20. Keserue, H.A.; Baumgartner, A.; Felleisen, R.; Egli, T. Rapid detection of total and viable Legionella pneumophila in tap water by immunomagnetic separation, double fluorescent staining and flow cytometry. *Microb. Biotechnol.* **2012**, *5*, 753–763. [CrossRef]

21. Bloemen, M.; Denis, C.; Peeters, M.; de Meester, L.; Gils, A.; Geukens, N.; Verbiest, T. Antibody-modified iron oxide nanoparticles for efficient magnetic isolation and flow cytometric determination of L. pneumophila. *Microchim. Acta* **2015**, *182*, 1439–1446. [CrossRef]

22. Tamer, U.; Gündoğdu, Y.; Boyacı, İ.H.; Pekmez, K. Synthesis of magnetic core–shell Fe3O4–Au nanoparticle for biomolecule immobilization and detection. *J. Nanopart. Res.* **2010**, *12*, 1187–1196. [CrossRef]

23. Roth, H.-C.; Schwaminger, S.P.; Schindler, M.; Wagner, F.E.; Berensmeier, S. Influencing factors in the co-precipitation process of superparamagnetic iron oxide nano particles: A model based study. *J. Magn. Magn. Mater.* **2015**, *377*, 81–89. [CrossRef]

24. Tang, X.; Nakata, Y.; Li, H.O.; Zhang, M.; Gao, H.; Fujita, A.; Sakatsume, O.; Ohta, T.; Yokoyama, K. The optimization of preparations of competent cells for transformation of E. coli. *Nucleic Acids Res.* **1994**, *22*, 2857–2858. [CrossRef]

25. Kralj, S.; Drofenik, M.; Makovec, D. Controlled surface functionalization of silica-coated magnetic nanoparticles with terminal amino and carboxyl groups. *J. Nanopart. Res.* **2011**, *13*, 2829–2841. [CrossRef]

26. Gao, F.; Cai, Y.; Zhou, J.; Xie, X.; Ouyang, W.; Zhang, Y.; Wang, X.; Zhang, X.; Wang, X.; Zhao, L.; et al. Pullulan acetate coated magnetite nanoparticles for hyper-thermia: Preparation, characterization and in vitro experiments. *Nano Res.* **2010**, *3*, 23–31. [CrossRef]

27. Schwaminger, S.P.; Bauer, D.; Fraga-García, P.; Wagner, F.E.; Berensmeier, S. Oxidation of magnetite nanoparticles: Impact on surface and crystal properties. *Cryst. Eng. Comm.* **2017**, *19*, 246–255. [CrossRef]

28. Bini, R.A.; Marques, R.F.C.; Santos, F.J.; Chaker, J.A.; Jafelicci, M. Synthesis and functionalization of magnetite nanoparticles with different amino-functional alkoxysilanes. *J. Magn. Magn. Mater.* **2012**, *324*, 534–539. [CrossRef]

29. Yu, S.; Chow, G.M. Carboxyl group (–CO$_2$H) functionalized ferrimagnetic iron oxide nanoparticles for potential bio-applications. *J. Mater. Chem.* **2004**, *14*, 2781–2786. [CrossRef]

30. Alp, E.; Aydogan, N. A comparative study: Synthesis of superparamagnetic iron oxide nanoparticles in air and N 2 atmosphere. *Colloids Surf. A* **2016**, *510*, 205–212. [CrossRef]

31. Karaagac, O.; Kockar, H.; Beyaz, S.; Tanrisever, T. A simple way to synthesize superparamagnetic iron oxide nanoparticles in air atmosphere: Iron ion concentration effect. *IEEE Trans. Magn.* **2010**, *46*, 3978–3983. [CrossRef]

32. McCarthy, S.A.; Davies, G.-L.; Gun'ko, Y.K. Preparation of multifunctional nanoparticles and their assemblies. *Nat. Prot.* **2012**, *7*, 1677–1693. [CrossRef] [PubMed]

33. Dodi, G.; Hritcu, D.; Draganescu, D.; Popa, M.I. Iron oxide nanoparticles for magnetically assisted patterned coatings. *J. Magn. Magn. Mater.* **2015**, *388*, 49–58. [CrossRef]

34. Mahadevan, S.; Gnanaprakash, G.; Philip, J.; Rao, B.P.C.; Jayakumar, T. X-ray diffraction-based characterization of magnetite nanoparticles in presence of goethite and correlation with magnetic properties. *Phys. E* **2007**, *39*, 20–25. [CrossRef]

35. Ma, M.; Zhang, Y.; Yu, W.; Shen, H.Y.; Zhang, H.Q.; Gu, N. Preparation and characterization of magnetite nanoparticles coated by amino silane. *Colloids Surf. A* **2003**, *212*, 219–226. [CrossRef]

36. Yamaura, M.; Camilo, R.L.; Sampaio, L.C.; Macêdo, M.A.; Nakamura, M.; Toma, H.E. Preparation and characterization of (3-aminopropyl)triethoxysilane-coated magnetite nanoparticles. *J. Magn. Magn. Mater.* **2004**, *279*, 210–217. [CrossRef]

37. Huang, H.-C.; Hsieh, T.-E. Highly stable precursor solution containing ZnO nanoparticles for the preparation of ZnO thin film transistors. *Nanotechnology* **2010**, *21*, 295707. [CrossRef]

38. Sun, W.; Sun, W.; Kessler, M.R.; Bowler, N.; Dennis, K.W.; McCallum, R.W.; Li, Q.; Tan, X. Multifunctional properties of cyanate ester composites with SiO_2 coated Fe_3O_4 fillers. *ACS Appl. Mater. Interfaces* **2013**, *5*, 1636–1642. [CrossRef]

39. Morhardt, C.; Ketterer, B.; Heißler, S.; Franzreb, M. Direct quantification of immobilized enzymes by means of FTIR ATR spectroscopy – A process analytics tool for biotransformations applying non-porous magnetic enzyme carriers. *J. Mol. Catal. B: Enzym.* **2014**, *107*, 55–63. [CrossRef]

40. Bloemen, M.; van Stappen, T.; Willot, P.; Lammertyn, J.; Koeckelberghs, G.; Geukens, N.; Gils, A.; Verbiest, T. Heterobifunctional PEG ligands for bioconjugation reactions on iron oxide nanoparticles. *PLoS ONE* **2014**, *9*, e109475. [CrossRef]

41. Zhang, S.; Zou, L.; Zhang, D.; Pang, X.; Yang, H.; Xu, Y. GoldMag nanoparticles with core/shell structure: Characterization and application in MR molecular imaging. *J. Nanopart. Res.* **2011**, *13*, 3867–3876. [CrossRef]

42. Caruso, F.; Furlong, D.N.; Ariga, K.; Ichinose, I.; Kunitake, T. Characterization of polyelectrolyte−protein multilayer films by atomic force microscopy, scanning electron microscopy, and Fourier transform infrared reflection−absorption spectroscopy. *Langmuir* **1998**, *14*, 4559–4565. [CrossRef]

43. Smidt, E.; Meissl, K. The applicability of Fourier transform infrared (FT-IR) spectroscopy in waste management. *Waste Manage.* **2007**, *27*, 268–276. [CrossRef]

44. Helm, D.; Naumann, D. Identification of some bacterial cell components by FT-IR spectroscopy. *FEMS Microbiol. Lett.* **1995**, *126*, 75–79. [CrossRef]

45. Bohmer, N.; Demarmels, N.; Tsolaki, E.; Gerken, L.; Keevend, K.; Bertazzo, S.; Lattuada, M.; Herrmann, I.K. Removal of cells from body fluids by magnetic separation in batch and continuous mode: Influence of bead size, concentration, and contact time. *ACS Appl. Mater. Interfaces* **2017**, *9*, 29571–29579. [CrossRef]

46. Xu, H.; Aguilar, Z.P.; Yang, L.; Kuang, M.; Duan, H.; Xiong, Y.; Wei, H.; Wang, A. Antibody conjugated magnetic iron oxide nanoparticles for cancer cell separation in fresh whole blood. *Biomaterials* **2011**, *32*, 9758–9765. [CrossRef]

47. Mobed, A.; Hasanzadeh, M.; Agazadeh, M.; Mokhtarzadeh, A.; Rezaee, M.A.; Sadeghi, J. Bioassays: The best alternative for conventional methods in detection of Legionella pneumophila. *Int. J. Biol. Macromol.* **2019**, *121*, 1295–1307. [CrossRef]

48. Delgado-Viscogliosi, P.; Simonart, T.; Parent, V.; Marchand, G.; Dobbelaere, M.; Pierlot, E.; Pierzo, V.; Menard-Szczebara, F.; Gaudard-Ferveur, E.; Delabre, K.; et al. Rapid method for enumeration of viable Legionella pneumophila and other Legionella spp. in water. *Appl. Environ. Microbiol.* **2005**, *71*, 4086–4096. [CrossRef]

49. LeChevallier, M.W. Occurrence of culturable Legionella pneumophila in drinking water distribution systems. *AWWA Wat. Sci.* **2019**, *1*, e1139. [CrossRef]

50. Montagna, M.T.; De Giglio, O.; Napoli, C.; Diella, G.; Rutigliano, S.; Agodi, A.; Auxilia, F.; Baldovin, T.; Bisetto, F.; Arnoldo, L.; et al. Control and prevention measures for legionellosis in hospitals: A cross-sectional survey in Italy. *Environ. Res.* **2018**, *166*, 55–60. [CrossRef]